JOURNAL OF SOLID STATE CHEMISTRY **140,** 233–241 (1998)
ARTICLE NO. SC987881

Magnetic Structures of the Rare-Earth Platinum Aluminides *R*PtAl (*R* = Ce, Pr, Nd)

H. Kitazawa,* A. Dönni,*,[1] L. Keller,† J. Tang,* F. Fauth,†,[2] and G. Kido*

*National Research Institute for Metals, Tsukuba, Ibaraki 305-0047, Japan; and †Laboratory for Neutron Scattering, ETH Zürich and Paul Scherrer Institute, CH-5232 Villigen PSI, Switzerland

Received December 18, 1997; revised May 4, 1998; accepted May 12, 1998

The rare-earth (*R*) platinum aluminides *R*PtAl crystallize in the orthorhombic TiNiSi-type structure (space group Pnma, *Z*=4), where magnetic rare-earth atoms form a network of chains parallel to the *a*-axis and parallel to the *b*-axis. Magnetic structures and phase transitions of *R*PtAl (*R* = Ce, Pr, Nd) compounds were investigated by systematic measurements of magnetic susceptibility, specific heat, and neutron diffraction on polycrystalline samples. The results reveal a large magnetocrystalline anisotropy and magnetic structures that are dominated by a ferromagnetic component parallel to one of the two chain directions: the *a*-axis for CePtAl and PrPtAl and the *b*-axis for NdPtAl. The complex magnetism of CePtAl with three successive magnetic phase transitions ($T_C = 5.9$ K, $T_2 = 4.3$ K, $T_3 = 2.5$ K) and two coexisting propagation vectors ($\mathbf{k}_1 = 0$ for $T \le T_C$, $\mathbf{k}_{2i} = [0, 0.46, 0]$ for $T_2 \le T \le T_C$, $\mathbf{k}_2 = [0, 1/2, 0]$ for $T \le T_2$) is confirmed to be exceptional among *R*PtAl compounds. PrPtAl has a nonmagnetic crystalline-electric field (CEF) ground-state singlet separated by 21 K from the first-excited state CEF singlet and magnetic exchange interactions are strong enough to induce long-range magnetic order (Curie temperature $T_C = 5.8$ K, propagation vector $\mathbf{k}_1 = 0$, magnetic group Pnm′a′, ordered saturation moment $m_1 = 1.00(7)\ \mu_B$). NdPtAl is a simple ferromagnet ($T_C = 19.2$ K, $\mathbf{k}_1 = 0$, Pn′ma′, $m_1 = 2.08(4)\ \mu_B$).

1. INTRODUCTION

Members of the ternary rare-earth (*R*) aluminides *RT*Al (*T* = Ni, Pd, Pt) crystallize in the hexagonal ZrNiAl-type or in the orthorhombic TiNiSi-type structure (1, 2). The ZrNiAl-type structure is found in *R*NiAl (*R* = all rare earth) and in *R*PdAl (*R* = light rare earth) compounds, whereas the TiNiSi-type structure is stable in *R*PdAl (*R* = heavy rare earth) and *R*PtAl (*R* = all rare earth) samples. Although there is no direct relationship between these two crystal structures, the nearest neighbor coordination polyhedra of the atoms are similar and subtle details must be responsible for the choice of the structure. For example for the *R*PdAl compounds the third root of the volumes $d = (V/Z)^{1/3}$ plotted versus the R^{3+} ionic radii lies on a fairly straight line through the structural phase transition (1).

*R*NiAl and *R*PdAl compounds with ZrNiAl-type structure have recently attracted considerable interest because magnetic order is characterized by *geometrical frustration* of magnetic moments (3–6). Magnetic rare-earth atoms form a Kagomé-like lattice in the hexagonal basal plane with triangular coordination symmetry and antiferromagnetic nearest neighbor coupling. In connection with a strong magnetocrystalline anisotropy, this gives rise to the formation of chains consisting of two-thirds of nonfrustrated magnetic moments, which are separated by the other one-third of frustrated magnetic moments with reduced size. An extreme case is CePdAl (5), where a coexistence of ordered moments (2/3, in the chains) and paramagnetic (disordered) moments (1/3, off the chains) on the Ce atoms has been found, despite all Ce atoms being located on crystallographically equivalent rare-earth sites.

The TiNiSi-type crystal structure (orthorhombic space group Pnma with all atoms on sites (4c)) of the *R*PtAl compounds is shown in Fig. 1. The crystallographic unit cell contains four magnetic atoms *R*(1), *R*(2), *R*(3) and *R*(4) which form a network of chains parallel to the *a*-axis (*R*(1)-*R*(4)-*R*(1)... and *R*(2)-*R*(3)-*R*(2)...) and parallel to the *b*-axis (*R*(1)-*R*(3)-*R*(1)... and *R*(2)-*R*(4)-*R*(2)...). First magnetic susceptibility experiments (1) on *R*PtAl compounds revealed ferromagnetism below the Curie temperatures T_c of 6 K (CePtAl), 8 K (PrPtAl), and 18.5 K (NdPtAl). For a ferromagnetic structure the magnetic unit cell has the same size as the crystallographic unit cell and the magnetic propagation vector is $\mathbf{k}_1 = 0$. A group theoretical symmetry analysis (7) of possible magnetic configurations for the case of space group Pnma, site (4c) and $\mathbf{k}_1 = 0$ yields the eight

[1]Corresponding author. Present address: Department of Physics, Niigata University, Niigata 950-2181, Japan. E-mail: donni@sc.niigata-u.ac.jp.

[2]Present address: Institute Laue-Langevin (ILL), F-38042 Grenoble, France.

0022-4596/98 $25.00

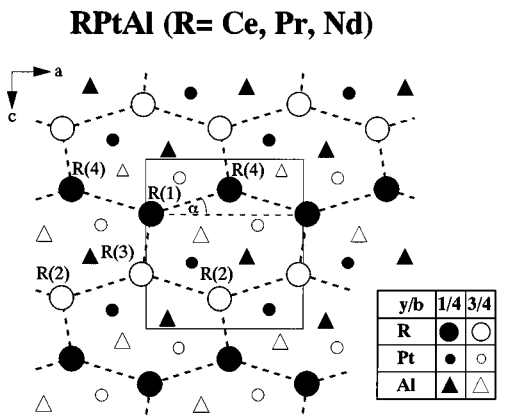

FIG. 1. TiNiSi-type crystal structure of *R*PtAl (*R* = Ce, Pr, Nd) compounds. Orthorhombic space group Pnma, No. 62, $Z = 4$, with all atoms on sites (4c).

one-dimensional irreducible representations $(\Gamma_1, \ldots, \Gamma_8)$ given in Table 1. Thus, for *R*PtAl systems one can expect to observe magnetic structures with a ferromagnetic component parallel to the *a*-axis (Γ_2), the *b*-axis (Γ_4), or the *c*-axis (Γ_3). Recently, a more detailed investigation on CePtAl including powder neutron diffraction experiments (8) indeed confirmed the presence of a ferromagnetic component parallel to the magnetically easy *a*-axis (representation Γ_2) but also revealed that magnetism in CePtAl is much more complex: CePtAl undergoes three successive magnetic phase transitions between 5.9 and 2.2 K with magnetic structures consisting of two coexisting partly incommensurate propagation vectors. Magnetic structures of CePtAl are unstable (9) in a magnetic field applied along the *c*-axis, e.g., perpendicular to the two chain directions.

Although geometrical frustration effects are not observed in *R*PtAl systems, the interesting results on CePtAl have motivated us to extend the investigation of magnetic properties of *R*PtAl compounds. In this paper we report on magnetic structures and phase transitions of CePtAl, PrPtAl, and NdPtAl investigated by systematic measurements of magnetic susceptibility, specific heat and neutron diffraction on polycrystalline samples.

TABLE 1

Group Theoretical Symmetry Analysis (7) of Possible Magnetic Configurations for the Case of Space Group Pnma, Site (4c), and Magnetic Propagation Vector $\mathbf{k_1} = 0$

(4c) positions				Magnetic moment configurations			
	x/a	y/b	z/c	F	C	A	G
(1)	x	1/4	z	+	+	+	+
(2)	$\bar{x} + 1/2$	3/4	$z + 1/2$	+	−	−	+
(3)	$\bar{x}$	3/4	$\bar{z}$	+	+	−	−
(4)	$x + 1/2$	1/4	$\bar{z} + 1/2$	+	−	+	−

Representation	Axial vectors			Magnetic group
	x	y	z	
Γ_1	.	C	.	Pnma
Γ_2	F	.	C	Pnm′a′
Γ_3	C	·	F	Pn′m′a
Γ_4	.	F	.	Pn′ma′
Γ_5	A	.	G	Pn′m′a′
Γ_6	.	G	.	Pn′ma
Γ_7	.	A	.	Pnma′
Γ_8	G	.	A	Pnm′a

Note. There are eight one-dimensional irreducible representations $(\Gamma_1, \ldots, \Gamma_8)$.

2. EXPERIMENTAL

Large amounts (about 25 g) of polycrystalline material of CePtAl, PrPtAl, NdPtAl and of the nonmagnetic reference compound LaPtAl were synthesized in four batches per sample by arc melting stoichiometric mixtures of the pure elements (La: 3N, Ce: 3N, Pr: 3N, Nd: 3N, Pt: 3N5, Al: 5N) in an argon atmosphere and were annealed at 900°C for 120 hr in high vacuum. For all samples the X-ray diffraction spectra could be completely indexed with the orthorhombic space group Pnma and there were no detectable impurity phase contributions.

The magnetic susceptibility $\chi \equiv M/H$ for *R*PtAl (*R* = Ce, Pr, Nd) was measured between 1.9 and 300 K in an applied field $H = 0.1\ T$ using a Quantum Design SQUID (superconducting quantum interference device) magnetometer. Field-cooled susceptibility data have been collected from fine powdered samples of about 100 mg which were fixed with paraffin to prevent reorientation.

Specific heat experiments between 1.5 and 30 K were performed for *R*PtAl (*R* = La, Ce, Pr, Nd) on bulk pieces of about 1 g using a semiadiabatic heat pulse method. The magnetic part of the specific heat, C_{mag}, was determined from the difference of specific heat of *R*PtAl (*R* = Ce, Pr, Nd) and of the nonmagnetic LaPtAl. The temperature dependence of the magnetic entropy $S_{mag}(T)$ has been obtained by the following integration:

$$S_{mag}(T) = \int_0^T [C_{mag}(\tau)/\tau]\, d\tau \qquad [1]$$

Neutron scattering experiments for *R*PtAl (*R* = Pr, Nd) were performed partly at the high-flux reactor of the Institute Laue-Langevin (ILL) in Grenoble, France, on the powder diffractometer D1A and on the triple-axis spectrometer IN3 and partly at the new neutron spallation source SINQ at the Paul Scherrer Institute (PSI) in Villigen, Switzerland, on the powder diffractometer DMC. For PrPtAl D1A

spectra were collected with a neutron wave-length $\lambda = 1.9114$ Å in the paramagnetic state at 15 K and in the magnetically ordered state at 1.5 K. The temperature dependence of magnetic Bragg peaks was studied on DMC with $\lambda = 2.562$ Å and some crystalline-electric field excitations were measured on IN3 with constant analyzer energy $E_F = 14.7$ meV. For NdPtAl D1A experiments to determine crystallographic and magnetic structures were done with $\lambda = 2.4783$ Å at 30 and 1.5 K. The temperature variation of magnetic Bragg peaks was measured on IN3, operated in the two-axis mode, with $\lambda = 2.45$ Å. Large amounts (PrPtAl: 16 g, NdPtAl: 18 g) of fine powder were filled under helium gas atmosphere into cylindrical vanadium containers (D1A) or aluminum containers (IN3 and DMC) and mounted in a standard ^{4}He orange cryostat. D1A and DMC diffraction patttern in the paramagnetic and magnetically ordered states were analyzed by the Rietveld method with the program FullProf (10) using the neutron scattering lengths published by Sears (11) and the relativistic magnetic form factors of Pr^{3+} and Nd^{3+} in dipolar approximation. The background was described with a five-order polynomial and peak-shape with a pseudo-Voigt function.

3. RESULTS

3.1. CePtAl

For the CePtAl single crystal measurements of specific heat (8), electrical resistivity (8), magnetic susceptibility (9), and high-field magnetization (9) have been reported so far. For the polycrystalline CePtAl sample previously studied by powder neutron diffraction (8) we have added in this work magnetic susceptibility and specific heat experiments. For convenience we present in this section our new data, together with relevant parts of the previously published results on CePtAl.

The parameters for the TiNiSi-type crystal structure of paramagnetic CePtAl at 11 K, obtained from a Rietveld refinement of powder neutron diffraction data, are given in Table 2. The temperature variation ($T < 12$ K) of magnetic susceptibility, specific heat, magnetic entropy and magnitudes of ordered Ce moments is displayed in Fig. 2. For the CePtAl single crystal magnetic phase transitions are observed at $T_C = 5.9$ K (second-order), $T_2 = 4.3$ K (first-order), and $T_3 = 2.2$ K (first-order). The specific heat shows a λ-type anomaly at T_C with an additional needle-like peak at T_2 (see Fig. 2). In the electrical resistivity steps appear at T_2 and T_3 (see Fig. 1 of (8)). Experiments on the polycrystalline CePtAl sample yielded identical values for T_C and T_2 and a slightly higher value for $T_3 = 2.5$ K. A strong increase in the magnetic susceptibility χ^{poly} near T_C indicates ferromagnetic ordering. Neutron diffraction experiments detected magnetic Bragg peaks corresponding to the commensurate propagation vectors $\mathbf{k_1} = 0$ (for $T \le T_C$) and $\mathbf{k_2} = [0, 1/2, 0]$ (for $T \le T_2$) and to the incommensurate propagation vector $\mathbf{k_{2i}} = [0, 0.46, 0]$ (for $T_2 \le T \le T_C$). T_3 is indicated by a weak anomaly in the intensity of m_2(Ce) with no change of magnetic propagation vector. Magnetic phase transitions and propagation vectors of CePtAl are summarized in Table 3.

TABLE 2

Crystal Structures (Orthorhombic Space Group Pnma, No. 62, Z = 4) and Selected Interatomic Distances for CePtAl (from (8)), PrPtAl, and NdPtAl Refined from Powder Neutron Diffraction Data

	CePtAl $T = 11$ K	PrPtAl $T = 1.5$ K	NdPtAl $T = 1.5$ K
a [Å]	7.2084(15)	7.1143(9)	7.0736(6)
b [Å]	4.4891(9)	4.4601(6)	4.4495(4)
c [Å]	7.7190(17)	7.7853(10)	7.7729(7)
V/Z [Å^3]	62.45(4)	61.76(3)	61.16(2)
b/a	0.6228(1)	0.6269(2)	0.6290(1)
c/a	1.0708(2)	1.0943(3)	1.0989(2)
R: x/a	0.0305(3)	0.0254(4)	0.0288(1)
R: y/b	1/4	1/4	1/4
R: z/c	0.3218(3)	0.3183(3)	0.3170(1)
R: B[Å^2]	0.4(1)	0.04(3)	0.00(3)
Pt: x/a	0.2861(1)	0.2815(1)	0.2807(1)
Pt: y/b	1/4	1/4	1/4
Pt: z/c	0.6128(1)	0.6129(1)	0.6122(1)
Pt: B [Å^2]	0.1(1)	0.04(3)	0.12(2)
Al: x/a	0.1446(4)	0.1479(4)	0.1451(3)
Al: y/b	1/4	1/4	1/4
Al: z/c	0.9328(4)	0.9343(4)	0.9336(3)
Al: B [Å^2]	0.3(1)	0.04(3)	0.26(4)
$d_{R(1)\text{-}R(3)}$ [Å]	3.578(5)	3.621(5)	3.634(2)
$d_{R(1)\text{-}R(4)}$ [Å]	3.771(2)	3.713(2)	3.687(1)
$d_{R(1)\text{-}R(3)}/d_{R(1)\text{-}R(4)}$	0.949(2)	0.975(2)	0.986(1)
α [°]	17.1(1)	16.6(1)	16.4(1)

Note. α: angle between $R(1)$-$R(4)$ direction and a-axis.

The magnetic susceptibility χ of the CePtAl single crystal (shown in Fig. 1 of (9)) exhibits a pronounced magnetic anisotropy. χ^a (measured parallel to the magnetically easy *a*-axis) nicely follows a Curie–Weiss law between 10 and 300 K with an effective magnetic moment $\mu^a_{eff} = 2.58\ \mu_B$ (close to the free ion value 2.54 μ_B for Ce^{3+}) and a Curie temperature $\Theta^a_p = 6.5$ K (close to $T_C = 5.9$ K), indicating ferromagnetic interactions. However, in χ^b, χ^c, as well as in χ^{poly} (measured for the polycrystalline sample) deviations from the Curie–Weiss law were observed up to room temperature (due to crystalline-electric-field effects) and there is no indication of ferromagnetic interactions. The magnetically hard axis changes from the *c*-axis ($T > 39$ K) to the *b*-axis ($T < 39$ K).

Specific heat data of the single crystal and of the polycrystalline sample were measured under similar experimental conditions with the same equipment. As illustrated in

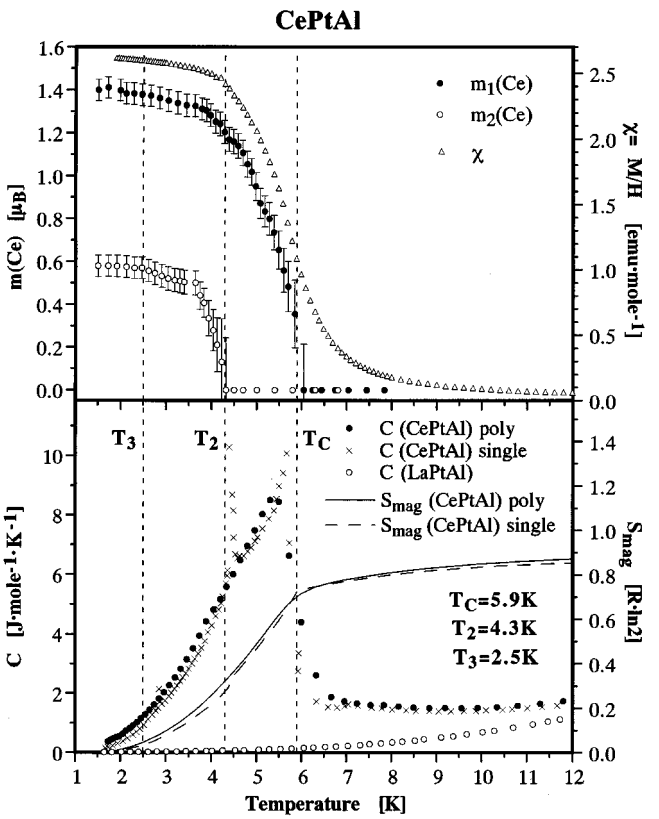

FIG. 2. Temperature dependence of magnitudes m_1(Ce), m_2(Ce) of ordered Ce moments, magnetic susceptibility χ, specific heat C, and magnetic entropy S_{mag} for polycrystalline CePtAl with a magnetic phase transitions at $T_C = 5.9$ K, $T_2 = 4.3$ K, and $T_3 = 2.5$ K. Also shown is the temperature variation of specific heat and magnetic entropy for the CePtAl single crystal.

Fig. 2 for decreasing temperature the increase of the specific heat at T_C appears steeper for the single crystal and the additional needle-like anomaly at T_2 could not be detected for the polycrystalline sample. Besides these two features the λ-type specific heat anomalies of the two samples look quite similar. For both samples the magnetic entropy S_{mag} released at T_C corresponds to about 72% of the value $R \cdot \ln 2$, the entropy of the crystalline-electric field ground-state doublet of CePtAl.

Powder neutron diffraction experiments revealed that magnetic structures of CePtAl consist of two coexisting Fourier components: $\mathbf{k_1} = 0$ and $\mathbf{k_{2i}} = [0, 0.46, 0]$ (for $T_2 \leq T \leq T_C$) and $\mathbf{k_1} = 0$ and $\mathbf{k_2} = [0, 1/2, 0]$ (for $T \leq T_2$). Magnetic Bragg intensity corresponding to $\mathbf{k_1}$ appears in the second-order phase transition at T_C and exhibits only a small anomaly at T_2 and no anomaly at T_3. For the $\mathbf{k_{2i}}$ component so far the spin arrangement and temperature dependence of magnetic Bragg intensity have not been investigated in detail. Magnetic structure data of CePtAl at 1.5 K are summarized in Table 4. The predominantly

TABLE 3
Magnetic Phase Transitions (at T_1, T_2, T_3), Propagation Vectors ($\mathbf{k_1}$, $\mathbf{k_{2i}}$, $\mathbf{k_2}$) for TbPdAl (from (15)), CePtAl, PrPtAl, and NdPtAl Compounds with TiNiSi-Type Crystal Structure

	TbPdAl	CePtAl	PrPtAl	NdPtAl
T_1 (T_C) [K]	43	5.9	5.8	19.2
T_2 [K]	22	4.3	—	—
T_3 [K]	—	2.2[a], 2.5[b]	—	—
$\mathbf{k_1}$ ($T \leq T_1$)	—	[0, 0, 0]	[0, 0, 0]	[0, 0, 0]
$\mathbf{k_{2i}}$ ($T_2 \leq T \leq T_1$)	[0.27, 0.48, 0]	[0, 0.46, 0]	—	—
$\mathbf{k_2}$ ($T \leq T_2$)	[0, 1/2, 0]	[0, 1/2, 0]	—	—
	m∥**b**	**m**⊥**b**	**m**⊥**b**	**m**∥**b**

Note. For T_3 slightly different values were obtained for single crystalline[a] and polycrystalline[b] CePtAl samples. Direction of the ordered moments (**m**) with respect to the b-axis (**b**).

ferromagnetic $\mathbf{k_1} = 0$ component gives rise to the spin arrangement shown in Fig. 5 of (8), which is similar to the one found in PrPtAl (see Section 3.2). Ordered Ce moments with a magnitude m_1(Ce) = 1.40(5) μ_B have a ferromagnetic component (F sequence) of 1.35(4) μ_B parallel to the a-axis and an antiferromagnetic component (C sequence) of 0.36(4) μ_B parallel to the c-axis. For the antiferromagnetic $\mathbf{k_2} = [0, 1/2, 0]$ component with m_2(Ce) = 0.58(5) μ_B the accuracy of the structure determination (shown in Fig. 6 of (8)) is limited by the weakness of observed magnetic neutron peaks. Furthermore, based on powder neutron diffraction data, it is impossible to determine the kind of coupling between the $\mathbf{k_1}$ and $\mathbf{k_2}$ components, which changes at T_3.

3.2. PrPtAl

For polycrystalline PrPtAl the temperature variation ($T < 28$ K) of magnetic susceptibility, specific heat,

TABLE 4
Magnetic Structures of CePtAl, PrPtAl, and NdPtAl at $T = 1.5$ K Determined by Powder Neutron Diffraction

	CePtAl	PrPtAl	NdPtAl
$\mathbf{k_1}$	[0, 0, 0]	[0, 0, 0]	[0, 0, 0]
m_1 [μ_B]	1.40(5)	1.00(7)	2.08(4)
Magnetic group	Pnm′a′	Pnm′a′	Pn′m′a
representation	Γ_2	Γ_2	Γ_4
μ_{1x} [μ_B]	$F = 1.35(4)$	$F = 0.95(6)$	0
μ_{1y} [μ_B]	0	0	$F = 2.08(4)$
μ_{1z} [μ_B]	$C = 0.36(4)$	$C = 0.28(6)$	0
β_1	15° ± 2°	16° ± 5°	—
$\mathbf{k_2}$	[0, 1/2, 0]	—	—
m_2 [μB]	0.58(5)	—	—

Note. β: angle between a-axis and the ordered magnetic moments with propagation vector (**k**) and magnitude (m).

magnetic entropy, and magnitude of ordered Pr moments is displayed in Fig. 3. Long-range magnetic order appears in a second-order phase transition at $T_C = 5.8$ K and there is no experimental evidence for further magnetic phase transitions. T_C is indicated by a change of slope in the specific heat curve and neutron diffraction experiments detected magnetic Bragg peaks for $T \leq T_C$. However, at T_C only 15% of the magnetic entropy $R \cdot \ln 2$ is released and PrPtAl exhibits strong short-range magnetic correlations up to temperatures of more than twice T_C. The small specific heat anomaly at T_C contains a tail extending towards 21 K, the temperature corresponding to the magnetic entropy $R \cdot \ln 2$. With increasing temperature the enhancement of the magnetic susceptibility χ^{poly}, reflecting ferromagnetic alignment of rare-earth spins, disappears much slower in PrPtAl than in CePtAl. For PrPtAl χ^{poly} reaches 74% of its saturation value at T_C, 10% at $2T_C$, and 5% at $3T_C$ (see Fig. 3). The corresponding values for χ^{poly} of CePtAl are 42% at T_C, 2% at $2T_C$, and 1% at $3T_C$ (see Fig. 2). The magnetic susceptibility χ^{poly} of PrPtAl follows a Curie–Weiss law between 120 and 300 K (see Fig. 4) with an effective magnetic moment $\mu_{eff} = 3.59(1)\ \mu_B$ (equal to the free ion value $3.58\ \mu_B$ of Pr^{3+}) and a negative Curie temperature $\Theta p = -(6.5 \pm 1.0)$ K with $|\Theta p| \approx T_C$. In the powder average magnetic exchange interactions of PrPtAl appear to be antiferromagnetic, despite the ferromagnetic component of the magnetic structure.

FullProf refinements of D1A neutron diffraction patterns of paramagnetic PrPtAl at 15 K and of magnetically ordered PrPtAl at 1.5 K are shown in Fig. 5. Magnetic Bragg peaks can all be indexed with the propagation vector $\mathbf{k_1} = 0$. A simultaneous refinement of crystal structure (148 inequivalent nuclear Bragg peaks) and magnetic structure (179 inequivalent magnetic Bragg peaks) was performed at 1.5 K in the range $10^\circ \leq 2\Theta \leq 147^\circ$ (step $\Delta 2\Theta = 0.05^\circ$, excluded region $112^\circ < 2\Theta < 114^\circ$, 2702 data points). The resulting parameters for crystal and magnetic structures at 1.5 K are given in Tables 2 and 4, respectively. The agreement values of the FullProf fit were $R_{wp} = 8.85\%$, $R_{exp} = 2.35\%$, $\chi^2 = (R_{wp}/R_{exp})^2 = 14.2$, $R_{I,N} = 7.33\%$ (for integrated nuclear intensities), and $R_{I,M} = 11.4\%$ (for integrated magnetic intensities). The magnetic structure of PrPtAl, illustrated in Fig. 6, corresponds to the representation Γ_2. Ordered Pr moments with a magnitude $m_1(\text{Pr}) = 1.00(7)\ \mu_B$ at 1.5 K have a ferromagnetic component (F sequence) of $0.95(6)\ \mu_B$ parallel to the *a*-axis and an antiferromagnetic component (C sequence) of $0.28(6)\ \mu_B$ parallel to the *c*-axis.

3.3. NdPtAl

For polycrystalline NdPtAl the temperature variation ($T < 28$ K) of magnetic susceptibility, specific heat, magnetic

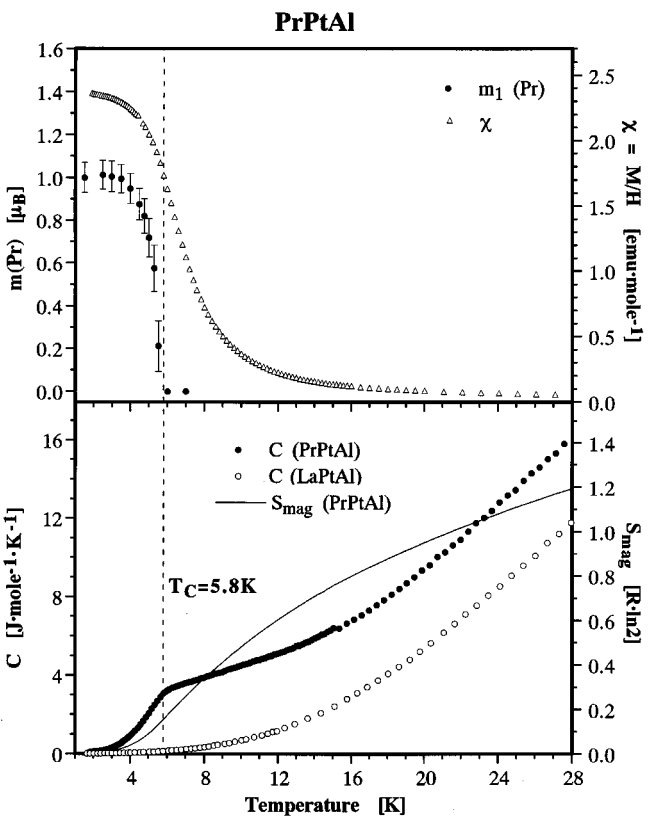

FIG. 3. Temperature dependence of magnitude m_1(Pr) of ordered Pr moments, magnetic susceptibility χ, specific heat C and magnetic entropy S_{mag} for polycrystalline PrPtAl with a magnetic phase transition at $T_C = 5.8$ K.

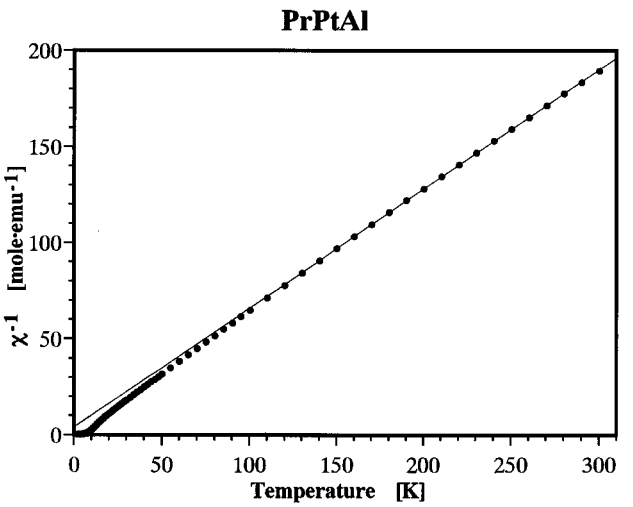

FIG. 4. Inverse magnetic susceptibility versus temperature for polycrystalline PrPtAl measured in the field-cooled mode in an applied external magnetic field $H = 0.1\ T$. The solid line indicates the fit to a Curie–Weiss law between 120 and 300 K.

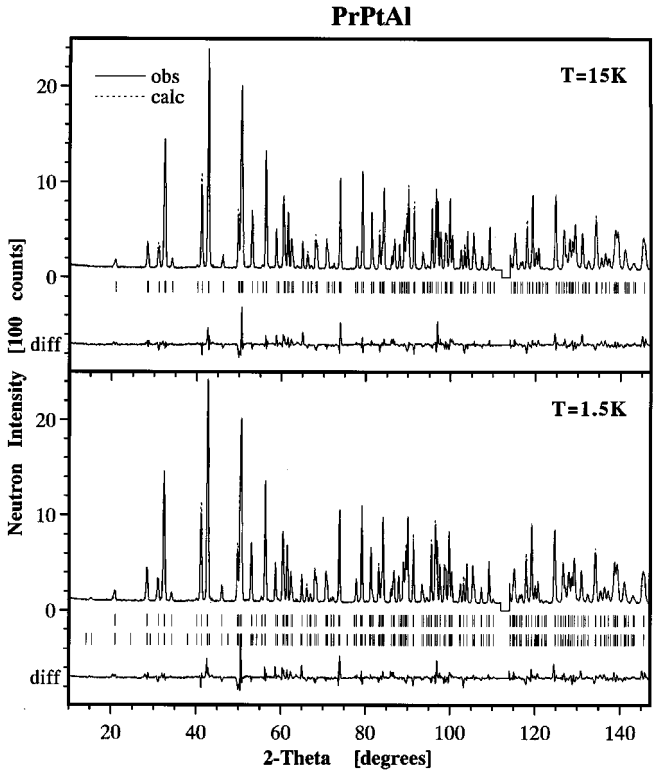

FIG. 5. Observed, calculated, and difference D1A neutron diffraction patterns ($\lambda = 1.9114$ Å) of paramagnetic PrPtAl at 15 K and magnetically ordered PrPtAl at 1.5 K. Vertical bars indicate positions of Bragg peaks for crystal and magnetic structures, respectively.

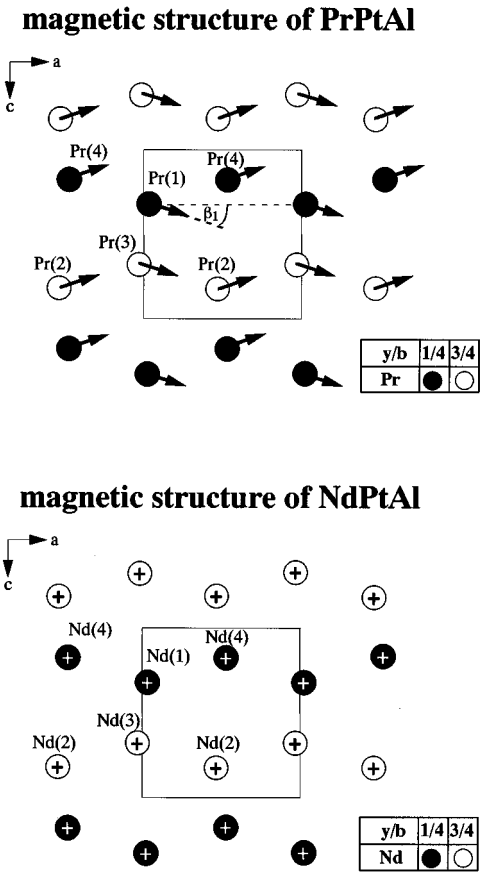

FIG. 6. Magnetic structures of PrPtAl and NdPtAl at 1.5 K. Ordered Pr moments (1.0 μ_B) are perpendicular and ordered Nd moments (2.1 μ_B) are parallel to the *b*-axis.

entropy, and magnitude of ordered Nd moments is displayed in Fig. 7. Long-range magnetic order appears in a second-order phase transition at $T_C = 19.2$ K, as indicated by a strong increase of the magnetic susceptibility χ^{poly}, by a λ-type specific heat anomaly containing a magnetic entropy close to $R \cdot \ln 2$, and by magnetic neutron Bragg intensity. In the magnetic susceptibility χ^{poly} deviations from the Curie–Weiss law, caused by crystalline-electric field effects, are detectable up to room temperature.

FullProf refinements of D1A neutron diffraction patterns of paramagnetic NdPtAl at 30 K and of magnetically ordered NdPtAl at 1.5 K are shown in Fig. 8. Magnetic Bragg peaks can all be indexed with the propagation vector $\mathbf{k_1} = 0$ and the same extinction rules for (hkl) reflections are valid for magnetic and crystal structures (e.g., for the site (4c) of space group Pnma). For example in contrast to CePtAl and PrPtAl for NdPtAl no magnetic intensity appears at the (1,0,0) Bragg peak (at $2\Theta = 20.2^\circ$ in Fig. 8). This Bragg reflection is forbidden by the symmetry of the TiNiSi-type crystal structure. A simultaneous refinement of crystal structure (74 inequivalent nuclear Bragg peaks) and magnetic structure (94 inequivalent magnetic Bragg peaks) was performed at 1.5 K in the range $10^\circ \leq 2\Theta \leq 151^\circ$ (step $\Delta 2\Theta = 0.05^\circ$, no excluded region, 2821 data points). The resulting parameters for crystal and magnetic structures of NdPtAl at 1.5 K are given in Tables 2 and 4, respectively. The agreement values of the FullProf fit were $R_{wp} = 4.21\%$, $R_{exp} = 2.72\%$, $\chi^2 = (R_{wp}/R_{exp})^2 = 2.40$, $R_{I,N} = 2.42\%$ and $R_{I,M} = 5.06\%$. NdPtAl adopts the simple ferromagnetic structure illustrated in Fig. 6 (representation Γ_4) with ordered Nd moments of $m_1(\text{Nd}) = 2.08(4)\ \mu_B$ at 1.5 K oriented parallel to the *b*-axis.

4. DISCUSSION

Magnetic properties of *R*PtAl compounds are affected by crystalline-electric-field (CEF) interactions. In the space group Pnma the rare-earth ions occupy the site (4c) with a low point symmetry (*.m.*), e.g., a mirror plane along the *b*-direction. Thus, for CePtAl the sixfold degenerate multiplet $^2F_{5/2}$ of Ce^{3+} is split by CEF interactions into three Kramers doublets. For PrPtAl the ninefold degenerate ground-state multiplet $^3H_4$ of Pr^{3+} decays into nine singlets

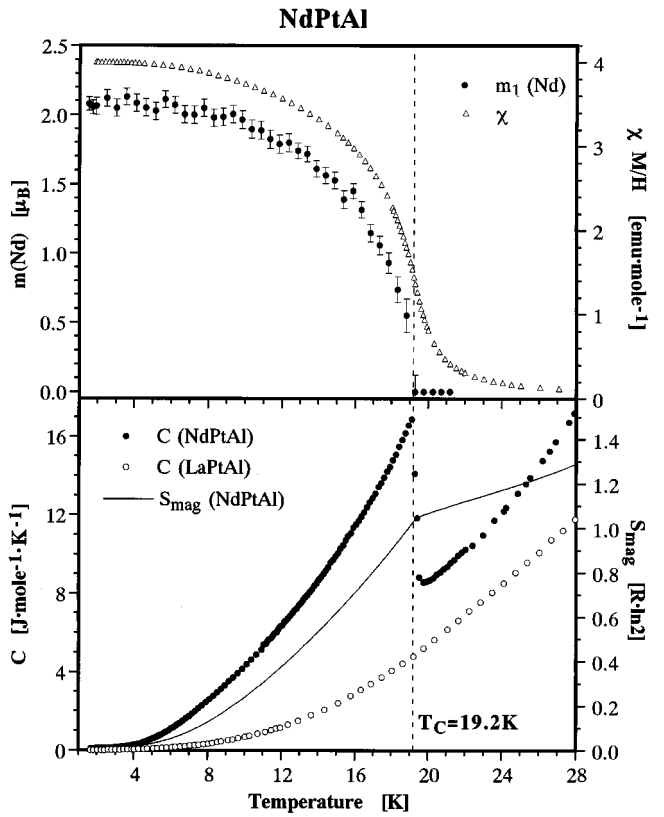

FIG. 7. Temperature dependence of magnitude m_1(Nd) of ordered Nd moments, magnetic susceptibility χ, specific heat C and magnetic entropy S_{mag} for polycrystalline NdPtAl with a magnetic phase transition at $T_C = 19.2$ K.

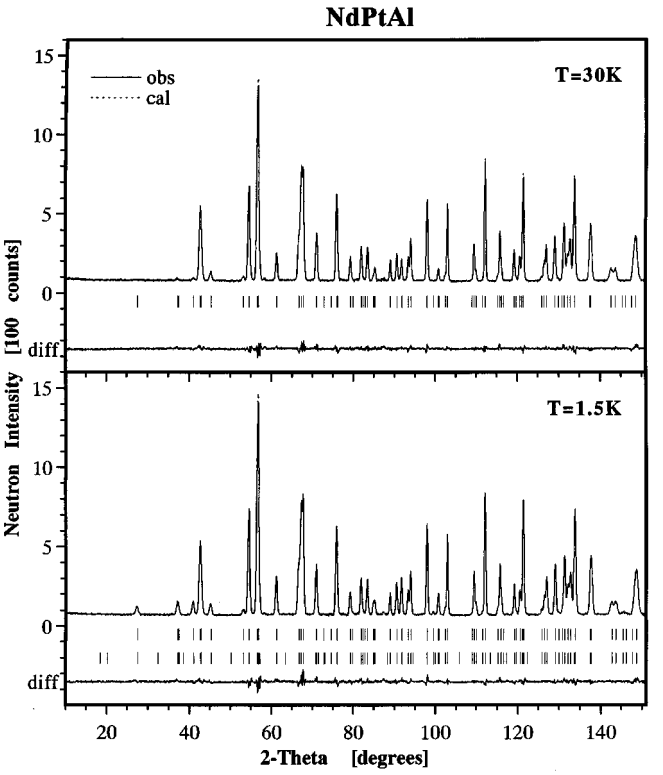

FIG. 8. Observed, calculated, and difference D1A neutron diffraction patterns ($\lambda = 2.4783$ Å) of paramagnetic NdPtAl at 30 K and magnetically ordered NdPtAl at 1.5 K. Vertical bars indicate positions of Bragg peaks for crystal and magnetic structures, respectively.

and for NdPtAl the tenfold degenerate ground-state multiplet $^4I_{9/2}$ of Nd^{3+} splits into five Kramers doublets.

For CePtAl and NdPtAl the λ-type specific heat anomalies, shown in Figs. 2 and 7, indicate that at the magnetic phase transition at T_C, a well-isolated CEF ground-state doublet, containing a magnetic entropy $R \cdot \ln 2$, is split by magnetic exchange interactions into two singlets. In CePtAl the 18% reduction of the magnetic entropy at T_C below the value $R \cdot \ln 2$, suggests a deviation of the Ce atoms from trivalency at low temperatures (possibly due to the Kondo effect) which, however, is weaker than, for example, in CePdAl (5).

To clarify the situation in PrPtAl, with nine CEF singlets, we have performed inelastic neutron scattering experiments. IN3 spectra of paramagnetic PrPtAl, displayed in Fig. 9, exhibit two excitations with large matrix elements at 1.8 meV (21 K) and at 6.0 meV (70 K) which, based on the observed **Q** and temperature dependence, can be identified to be both ground-state CEF transitions. Intensities of CEF transitions are decreasing with increasing scattering vector **Q** due to the magnetic form factor, and their temperature dependence is governed by Boltzman statistics. In PrPtAl the CEF ground-state singlet is separated by 21 K from the first excited-state CEF singlet, since 21 K corresponds, on one hand, to the energy of the CEF transition observed by inelastic neutron scattering (see Fig. 9) and, on the other hand to the temperature where the magnetic entropy $R \cdot \ln 2$, of two singlets, is released (see Fig. 3). In our experiments we have not attempted to determine the energies of all higher excited-state CEF singlets of PrPtAl. The particular shape of the specific heat anomaly of PrPtAl shown in Fig. 3 illustrates how magnetic exchange interactions are strong enough to overcome the CEF splitting of 21 K and to induce long-range magnetic order at $T_C = 5.8$ K. The presence of strong short-range magnetic correlations above T_C indicates that the ferromagnetic alignment along the magnetically easy *a*-axis (see χ versus T in Fig. 3) develops at higher temperatures than the coupling along the magnetically harder *b*-axis. The existence of an ordered magnetic state in a system with a nonmagnetic ground-state depends on a sensitive balance between the exchange interaction (which promotes the ordered state) and the CEF interaction (which tends to promote paramagnetism). In singlet ground-state systems the condition for the occurrence of

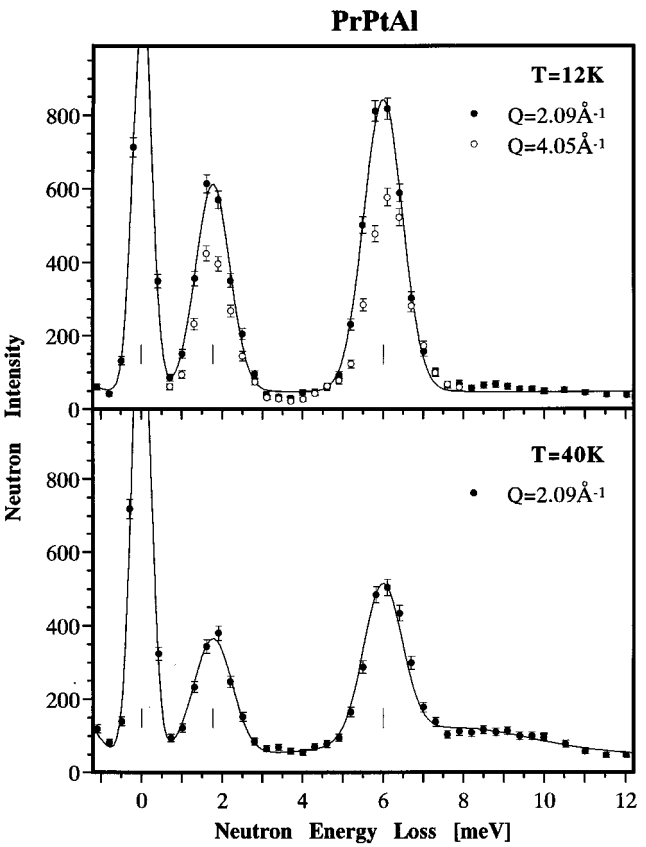

FIG. 9. IN3 energy spectra at 12 and 40 K of neutrons scattered from polycrystalline PrPtAl for constant momentum transfers $Q = 2.09$ Å^{-1} and 4.05 Å^{-1} and fixed analyzer energy $E_F = 14.7$ meV. The curves correspond to fits of the total scattering of the $Q = 2.09$ Å^{-1} measurements. Ground-state CEF excitations appear at 1.8 meV (21 K) and at 6.0 meV (70 K). The intensity near 8.8 meV indicates an excited-state CEF transition.

long-range magnetic order is given (12) by

$$J(0) \geq \Delta/4\alpha^2\,, \qquad [2]$$

where $J(0)$ is the molecular-field parameter and α is the matrix element for the dipole transitions between the singlet ground-state and the next higher level energetically separated by Δ. Examples of exchange-induced magnetic order are orthorhombic PrPtAl ($T_C = 5.8$ K) for a singlet-singlet CEF splitting and the cubic compounds Pr_3Tl ($T_C = 11$ K, (13)) and Pr_3Se_4 ($T_C \approx 15$ K (14)) for a singlet–triplet CEF splitting.

In RPtAl compounds CEF interactions induce a strong magnetic anisotropy (evidence are the magnetic susceptibility data of the CePtAl crystal (9) and the strong short-range magnetic correlations above T_C in PrPtAl) with a large overall CEF splitting of about 300 K or more (indicated by the deviations of the magnetic susceptibility curves of polycrystalline CePtAl and NdPtAl from the Curie–Weiss law) and give rise to remarkable reductions of the ordered saturation magnetic moments m_1 (CePtAl: 1.40(5) μ_B; PrPtAl: 1.00(7) μ_B; NdPtAl: 2.08(4) μ_B) below the free ions values gJ (Ce^{3+}: 2.14 μ_B; Pr^{3+}: 3.20 μ_B; Nd^{3+}: 3.27 μ_B). The direction of the ordered moments is determined by the magnetically easy axis of the low-lying CEF states to be either perpendicular (CePtAl, PrPtAl) or parallel (NdPtAl) to the *b*-axis, the direction of highest symmetry in the TiNiSi-type structure. Furthermore, magnetic susceptibility data on CePtAl and PrPtAl give evidence that magnetic exchange interactions are highly anisotropic: ferromagnetic along the *a*-axis and antiferromagnetic along *b*- and/or *c*-directions.

Magnetic structures of CePtAl, PrPtAl, and NdPtAl at 1.5 K are compared in Table 4. All compounds have a propagation vector $\mathbf{k_1} = 0$ and a second coexisting propagation vector is observed only for CePtAl. In the following we compare the $\mathbf{k_1}$ components of the magnetic structures, which are dominated by a ferromagnetic component along one of the two chain directions: the *a*-axis for CePtAl and PrPtAl (representation Γ_2) and the *b*-axis for NdPtAl (representation Γ_4). The magnetic moment arrangement for PrPtAl (equal to CePtAl) is plotted in Fig. 6. Within experimental uncertainty the value α (angle between *R*(1)–*R*(4) direction and *a*-axis; see Table 2 and Fig. 1) turns out to be equal to β_1 (the angle between ordered magnetic moments and the *a*-axis; see Table 4 and Fig. 6) which implies that at all *R* sites (*R* = Ce, Pr) the ordered moments are oriented parallel or antiparallel to directions determined by *R*-*R* second-nearest neighbors (e.g., *R*(1) and *R*(4)). Along the *R*-*R* nearest neighbors chains, the *b*-direction, ordered moments are coupled ferromagnetically. Also shown in Fig. 6 is the simple ferromagnetic structure of NdPtAl with ordered Nd moments parallel to the *b*-axis. For the $\mathbf{k_1}$ components of RPtAl (Ce, Pr, Nd) our experiments confirm that the direction of the ordered moments is temperature independent below T_C.

Low-temperature crystallographic structures of CePtAl, PrPtAl, and NdPtAl are compared in Table 2. The well-known lanthanide contraction results in a systematic decrease of the lattice constants *a*, *b*, *c* and of the volumes V/Z with increasing atomic number. This expected behavior, however, is in contrast to the systematic increase found for the ratios b/a and c/a. *R*-*R* distances are found to be generally smaller in the chains parallel to the *b*-axis ($d_{R(1)\text{-}R(3)}$) than in the chains parallel to the *a*-direction ($d_{R(1)\text{-}R(4)}$). From CePtAl to NdPtAl our data reveal a systematic decrease for the distance $d_{R(1)\text{-}R(4)}$ (in agreement with the decrease of the lattice constant *a*) and a systematic increase for the distance $d_{R(1)\text{-}R(3)}$ (in contrast to the decrease of the lattice constant *b*). Also for the *R*PtAl (*R* = Ce, Pr, Nd, Sm, Gd, Tb, Dy, Ho, Er, Tm, Lu) compounds the third root of the volumes $d = (V/Z)^{1/3}$ plotted versus the R^{3+} ionic radii lies on a straight line (1) with the same slope as the corresponding straight line for the *R*PdAl (*R* = Ce, Pr, Nd, Sm,

Gd, Tb, Dy, Ho, Er, Tm, Lu) systems. The slightly smaller d values for the Pt compounds demonstrate the slightly smaller size of the Pt atoms as compared with the Pd atoms, which among others is responsible for the change in the structure type.

For TbPdAl presently under investigation (15) single-phase samples were successfully prepared both in the orthorhombic TiNiSi-type crystal structure (stable low-temperature modification) and in the hexagonal ZrNiAl-type crystal structure (metastable high-temperature modification). Reflecting again the very close relationship of the two crystal structures, both modifications undergo two successive magnetic phase transitions with the same transition temperatures but effects of geometrical frustration are observed only in hexagonal TbPdAl. Magnetic properties of orthorhombic TbPdAl (with $d_{R(1)\text{-}R(3)} = 3.581(4)$ Å and $d_{R(1)\text{-}R(4)} = 3.615(3)$ Å) are also included in Table 3. The appearance of the magnetic propagation vector $\mathbf{k_2} = [0, 1/2, 0]$ below T_2 is connected with an intermediate incommensurate propagation vector $\mathbf{k_{2i}} = [0.27, 0.48, 0]$ ($T_2 \leq T \leq T_1$). In the TiNiSi-type crystal structure the propagation vector $\mathbf{k_1} = 0$ corresponds to the smallest possible magnetic unit cell and $\mathbf{k_2} = [0, 1/2, 0]$ to the second smallest possible magnetic unit cell. $\mathbf{k_1}$ is found for PrPtAl and NdPtAl with larger values for the distance $d_{R(1)\text{-}R(3)}$, whereas $\mathbf{k_2}$ (and $\mathbf{k_{2i}}$) appear in TbPdAl with a smaller value of $d_{R(1)\text{-}R(3)}$. But for samples with the TiNiSi-type structure the *coexistence* of the two most common *commensurate* propagation vectors $\mathbf{k_1}$ and $\mathbf{k_2}$ is rare and makes magnetism in CePtAl especially interesting. By powder neutron diffraction experiments it is impossible to completely solve the complex magnetic structures of CePtAl. For more detailed information about the coupling of the two Fourier components results of future single-crystal experiments of magnetic field or pressure dependence of magnetic neutron intensities of CePtAl must be awaited.

In summary we have presented systematic measurements of magnetic susceptibility, specific heat, and neutron diffraction to investigate magnetic structures and phase transitions of polycrystalline *R*PtAl (R = Ce, Pr, Nd) compounds. The results confirm that the complex magnetic structures of CePtAl are exceptional among *R*PdAl and *R*PtAl compounds with TiNiSi-type structure. PrPtAl has a nonmagnetic CEF ground-state singlet and long-range magnetic order is induced by magnetic exchange interactions. NdPtAl is a simple ferromagnet.

ACKNOWLEDGMENTS

We are indebted to P. Fischer for stimulating discussions and to M. Zolliker for assistance in the IN3 neutron scattering experiments. Financial support of the neutron scattering experiments by the Swiss National Science Foundation is gratefully acknowledged.

REFERENCES

1. F. Hulliger, *J. Alloys Compounds* **196,** 225 (1993).
2. F. Hulliger, *J. Alloys Compounds* **218,** 44 (1995).
3. G. Ehlers and H. Maletta, *Z. Phys. B* **99,** 145 (1996).
4. G. Ehlers and H. Maletta, *Z. Phys. B* **101,** 317 (1996).
5. A. Dönni, G. Ehlers, H. Maletta, P. Fischer, H. Kitazawa, and M. Zolliker, *J. Phys.: Condens. Matter* **8,** 11213 (1996).
6. G. Ehlers, C. Geibel, F. Steglich, and H. Maletta, *Z. Phys. B* **104,** 393 (1997).
7. E. F. Bertaut, *Acta Crystallogr. A* **24,** 217 (1968).
8. A. Dönni, H. Kitazawa, P. Fischer, J. Tang, M. Kohgi, Y. Endoh, and Y. Morii, *J. Phys.: Condens. Matter* **7,** 1663 (1995).
9. H. Kitazawa, S. Nimori, J. Tang, F. Iga, A. Dönni, T. Matsumoto, and G. Kido, *Physica B* **237/238,** 212 (1997).
10. J. Rodriguez-Carvajal, *Physica B* **192,** 55 (1993).
11. V. F. Sears, *Neutron News* **3,** 26 (1992).
12. B. R. Cooper, "Magnetic Properties of Rare Earth Metals" (R. J. Elliott, Ed.), p.17. Plenum, London, 1972.
13. K. Andres, E. Bucher, S. Darack, and J. P. Maita, *Phys. Rev. B* **6,** 2716 (1972).
14. E. Bucher, K. Andres, F. J. di Salvo, J. P. Maita, A. C. Gossard, A. S. Cooper, and G. W. Hull, *Phys. Rev. B* **11,** 500 (1975).
15. A. Dönni and H. Kitazawa, unpublished results